

Interacting random-field dipole defect model for heating in semiconductor-based qubit devices

Yujun Choi  and Robert Joynt ^{*}*Department of Physics, University of Wisconsin–Madison, Madison, Wisconsin 53706, USA* (Received 4 August 2023; revised 10 January 2024; accepted 17 January 2024; published 14 February 2024; corrected 22 July 2024)

Semiconductor qubit devices suffer from the drift of important device parameters as they are operated. The most important example is a shift in qubit operating frequencies. This effect appears to be directly related to the heating of the system as gate operations are applied. We show that the main features of this phenomenon can be explained by the two-level systems that can also produce charge noise if these systems are considered to form an interacting random-field glass. The most striking feature of the theory is that the frequency shift can be nonmonotonic in temperature. The success of the theory and the questions it raises considerably narrow the possible models for the two-level systems.

DOI: [10.1103/PhysRevResearch.6.013168](https://doi.org/10.1103/PhysRevResearch.6.013168)

I. INTRODUCTION

There has been considerable progress in semiconductor quantum computing, with significant strides in scaling up and in gate fidelities [1,2]. The chief difficulty is decoherence due to the fact that the qubits sit in a noisy environment, with charge noise being one of the most important. The charge noise is often modeled as random telegraph noise (RTN). This gives a good explanation of the low-frequency noise in quantum point contacts [3,4], in Hall bars [5], and in quantum dots [4]. RTN is seen in GaAs/Al_xGa_{1-x} heterostructures [6–8], Si/SiGe structures [4], and the Si/SiO₂ interface [9] and seems to be particularly associated with the regions near gates [8,10]. The key point for our purpose here is that two-level systems (TLSs) with a fluctuating electric dipole moment are the only natural explanation of RTN. RTN, together with the assumption of uniform distribution of barrier heights, also provides a natural explanation of the 1/*f* noise that is seen in quantum dots and many other solid-state systems [11]. There have been extensive characterizations of the noise spectrum [12,13] and the spatial correlations in the noise [14,15] in different devices. These observations can help in the elucidation of the nature of TLSs, but the data are not currently sufficient to pin things down precisely.

Another problem, at first sight quite separate, that interferes with qubit operation is the pulse-induced resonance shift (PIRS). This is a shift in the operating frequency of the qubits as a computation proceeds. It is highly problematic since continual recalibration of the system is not practical. Quadrature control [16] and prepulsing [17] can mitigate but not eliminate this issue. PIRS was recently the focus of an intensive experimental study [18].

Here we propose that the source of PIRS is also a group of TLSs, perhaps the same group that gives charge noise. Hence, detailed observations of PIRS may provide additional insight into the microscopic origin of the noise. We proceed in the time-honored fashion of proposing a phenomenological model that explains the data and then seeing what constraints the model places on the underlying physics of the system.

Let us take a concrete situation in which the system is in a resting state at a low temperature *T* for times *t* < 0 and the operations, which involve microwave pulses that feed energy into the system, begin at *t* = 0 and end at some later time *t_f*. PIRS is a time-dependent shift $\Delta f(t)$, with $\Delta f(t = 0) = 0$ by definition. Δf is a function of time that ultimately reverts to the base state sometime after the operations have ceased. PIRS appears to be rather ubiquitous in semiconductor qubits, but there is considerable variability in how it manifests itself. Early observations found positive shifts ($\Delta f \geq 0$) of the order of a few megahertz [17]. The magnitude of the shift was an increasing function of the energy injected by the pulses. It also depended on the details of the electron wave functions in the dots, for example, on the dot occupations. The megahertz magnitude of the shifts is fairly typical for quantum dot qubits. It generally occurs on top of the operating frequency *f*, which is about 10–20 GHz. Importantly, Δf can also be negative [16,19]. The decay time after *t_f* varies in the dot systems, with values from 0.5 ms [1] to 38 μs [19] having been observed. PIRS also occurs in donor-based qubit systems [20], although $|\Delta f|$ is much smaller, of the order of tens of kilohertz. Effects of a similar magnitude are seen in flip-flop qubits [21]. In this work we concentrate on experiments in dots, but we expect the theory to apply more broadly.

Our interpretation is based on the fact that dot and donor systems share the feature that the qubit operating frequency depends on the spatial position of the qubit. The arbitrary sign of Δf then suggests that a change in the electric field on the qubit is the origin of PIRS. Experimentally, it now appears to be clear that PIRS is essentially a thermal heating effect rather than a mechanical effect [1,18]. This is also supported by the characteristic return to a base state, most naturally interpreted as a return to thermal equilibrium. The most striking feature

^{*}rjjoynt@wisc.edu

of the results is that the magnitude of $\Delta f(T)$ is typically not monotonic in temperature T , instead rising to a maximum at about 200–300 mK and then decreasing [18].

We focus on explaining the T dependence of PIRS rather than attempting to relate it to the pulse sequences and amplitudes. Doing the latter would require a detailed calculation of the heat flow in the system. That would be very challenging, since phonon mean free paths are comparable to the dimensions of device features, rendering the usual macroscopic theory of heat conduction inapplicable [22,23].

II. MODEL

To explain these observations, we introduce a model based on the charged TLSs that are known to exist in these devices and that, in fact, are also responsible, at least in part, for the decoherence of the qubits. These charged defects or traps are modeled as a collection of N fluctuating electric dipoles. The j th dipole fluctuates between states $s_j \mathbf{p}_j$, where $s_j = \pm 1$ and \mathbf{p}_j is a fixed vector for each j . The model is Ising-like in that only two antiparallel directions for any single dipole are allowed, but as we will explain further below, the axis for the dipoles may not always be the same. For simplicity we assume that the dipoles all have the same magnitude: $|\mathbf{p}_j| = p_0$. This is reasonable if all the TLSs have the same physical origin. The dipoles can have a nonzero equilibrium moment which is random in direction, and they interact via the long-range Coulomb interaction. We call this the interacting random-field glass model (IRGM). Somewhat similar models have been introduced to understand charge noise (rather than equilibrium fields) in dot systems [24] and also in the context of superconducting qubit systems to explain fluctuations in the relaxation time T_1 [25,26].

The electric field $\langle \mathbf{F}_q \rangle$ on a qubit at the origin of coordinates is

$$\langle \mathbf{F}_q \rangle = \frac{1}{4\pi\epsilon} \sum_{j=1}^N \langle s_j \rangle \frac{3(\mathbf{p}_j \cdot \mathbf{r}_j) \mathbf{r}_j - \mathbf{p}_j |\mathbf{r}_j|^2}{|\mathbf{r}_j|^5} \equiv \sum_{j=1}^N \langle s_j \rangle \mathbf{F}_j. \quad (1)$$

The angle brackets indicate a thermal average. In the devices in question, the qubit operation frequency depends linearly on the electric field at its position. The frequency is a quasiequilibrium quantity, so $\langle \mathbf{F}_q \rangle$ is the object of interest for our purposes. The relation between field and frequency is platform dependent. In the setup of Refs. [1,16,17], $\langle \mathbf{F}_q \rangle$ causes the displacement of the spin qubit in a magnetic field gradient, so that the flipping of the TLS moves the qubit in the field gradient, changing the physical magnetic field on the spin. We can therefore regard $\langle \mathbf{F}_q \rangle$ as an effective magnetic field. Further details are given in Appendix A. In the flip-flop qubit architecture, motion of the qubit caused by $\langle \mathbf{F}_q \rangle$ would change the hyperfine coupling or the g factor [27]. In all cases the displacement changes the qubit operating frequency. The qubit frequency is $f(T) = f_0 + \mathbf{c}_q \cdot \langle \mathbf{F}_q \rangle(T=0) + \Delta f(T)$, where f_0 is the T -independent part from the applied magnetic field, $\langle \mathbf{F}_q \rangle(T=0) \neq 0$ is a constant that comes from the ground state configuration of the TLS, and $\Delta f(T)$ is the PIRS effect, and all the T dependence of f comes from it. Thus, $\Delta f(T) = \mathbf{c}_q \cdot [\langle \mathbf{F}_q \rangle(T) - \langle \mathbf{F}_q \rangle(T=0)]$ is the quantity of interest.

Introducing \mathbf{c}_q , the frequency susceptibility, in this way embodies the assumption of linearity of the dependence of Δf on the static electric field. \mathbf{c}_q depends on the particular type of qubit and the position of the qubit in the device. Its direction is determined by the condition that the effective magnetic field produced by $\langle \mathbf{F}_q \rangle$ (see Appendix A) should be parallel to the applied magnetic field.

The Hamiltonian of the TLS in our model contains a random-field term H_r and an interaction term H_{int} :

$$H = H_r + H_{\text{int}} = -p_0 \sum_{j=1}^N s_j \mathbf{E}_j \cdot \hat{\mathbf{p}}_j + \frac{p_0^2}{8\pi\epsilon} \sum_{j \neq k=1}^N s_j s_k V_{jk}.$$

Here

$$V_{jk} = \frac{3(\hat{\mathbf{p}}_j \cdot \hat{\mathbf{p}}_k) |\mathbf{r}_j - \mathbf{r}_k|^2 - \hat{\mathbf{p}}_j \cdot (\mathbf{r}_j - \mathbf{r}_k) \hat{\mathbf{p}}_k \cdot (\mathbf{r}_j - \mathbf{r}_k)}{|\mathbf{r}_j - \mathbf{r}_k|^5}.$$

The random effective electric fields \mathbf{E}_j , if interpreted in a double-well picture of the TLS, are related to the energy asymmetry (“detuning”) of the two wells. However, the physical origin of \mathbf{E}_j may not be the same in all cases. For example, they could be actual external electric fields coming from gate electrodes, strain fields, asymmetric microscopic defects, etc. For our purposes they are considered to be phenomenological parameters that must be fit since they are very difficult to estimate in the absence of a real microscopic model. We expect N to be a number in the range of perhaps 10 to 100 and to be sample dependent [12]. The dipoles may well be the same TLSs that give rise to the noise in the system, but here we are interested in their equilibrium behavior, not their fluctuations. This assumes that measurement of PIRS takes place over a time interval longer than the characteristic switching times of the TLSs. However, the intersection of the set of TLSs that causes qubit dephasing and the set that causes PIRS need not be complete.

III. NONMONOTONICITY OF PIRS

The T dependence of $\langle \mathbf{F}_q \rangle$ in a noninteracting model with $H_{\text{int}} = 0$ is already interesting, so we discuss it in detail. In this case the problem is exactly solvable, once the positions of the dipoles are specified: $\langle s_j \rangle = \text{sgn}(\hat{\mathbf{p}}_j \cdot \mathbf{E}_j) \tanh(p_0 \hat{\mathbf{p}}_j \cdot \mathbf{E}_j / k_B T)$. $\langle s_j \rangle$ has a definite sign at $T = 0$, but eventually, $\langle s_j \rangle \rightarrow 0$ as $T \rightarrow \infty$. We can identify a turnoff temperature $T_j = p_0 |\mathbf{E}_j| / k_B$ for each TLS. Substituting the form of $\langle s_j \rangle$ into Eq. (1) and performing the sum give the equilibrium electric field $\langle \mathbf{F}_q \rangle(T)$ at the qubit.

To understand the qualitative T dependence of $\langle \mathbf{F}_q \rangle$ in the IRGM we begin with $T = 0$. We divide the TLSs into two groups. In the set S^+ we have the indices j for which $\langle \mathbf{F}_q \rangle(T=0) \cdot \mathbf{F}_j \langle s_j \rangle(T=0) > 0$, while in group S^- we have the indices j for which $\langle \mathbf{F}_q \rangle(T=0) \cdot \mathbf{F}_j \langle s_j \rangle(T=0) < 0$. That is, the dipoles in S^+ are aligned with the ground state resultant field, while those in S^- are antialigned. The electric field at the qubit is the result of a random walk of the vectors $\langle s_j \rangle \mathbf{F}_j$ with the resultant vector

$$\langle \mathbf{F}_q \rangle = \sum_{j \in S^+} \langle s_j \rangle \mathbf{F}_j + \sum_{j \in S^-} \langle s_j \rangle \mathbf{F}_j. \quad (2)$$

The vectors in group S^+ are in the direction of the final result of the walk, while those in group S^- are in the opposite direction. Due to the randomness in the asymmetry, the various components of the walk turn off at different temperatures, and there will be some average turnoff temperature T^+ for group S^+ and a different average turnoff temperature T^- for group S^- . We now increase T from zero. If $T^+ > T^-$, then the total field strength $|\langle \mathbf{F}_q \rangle|$ will first increase and eventually vanish when $T \gg T^+$. In this case we have a nonmonotonic T dependence of the field strength $|\langle \mathbf{F}_q \rangle|$, a rather surprising result. T^+ and T^- are not expected to be very different if the dipoles have the same physical structure, but even in this case the relatively small value of N implies that random fluctuations will make $T^+ \neq T^-$. If $T^+ < T^-$, then the total field strength $|\langle \mathbf{F}_q \rangle|$ will decrease as the dominant dipoles turn off and eventually vanish when $T \gg T^-$. If there is a gross mismatch between T^+ and T^- , then one or more of the components of $\langle \mathbf{F}_q \rangle$ could even reverse sign, but overall, we would expect a monotonic decrease. The relative magnitudes of $|\sum_{j \in S^+} \langle s_j \rangle \mathbf{F}_j|$ and $|\sum_{j \in S^-} \langle s_j \rangle \mathbf{F}_j|$ are also important. If $|\sum_{j \in S^+} \langle s_j \rangle \mathbf{F}_j|$ dominates, then there is little cancellation in the sum, and the nonmonotonic behavior will be suppressed. If the fields from S^+ and S^- are comparable, then nonmonotonicity is more likely.

Now we turn to the effects of interactions. Dipolar interactions are always antiferromagnetic after averaging over the directions of the separation vector. (This may be seen by noting that the second term in V_{jk} vanishes when averaged over the directions of $\mathbf{r}_j - \mathbf{r}_k$, leaving the first term, which is proportional to $\hat{p}_j \cdot \hat{p}_k$.) This favors depolarization—a smaller net moment $|\langle \mathbf{P} \rangle| = |\sum_j \langle s_j \rangle \mathbf{p}_j|$. If the TLSs are located on one side of the qubit, then the correlation between $|\langle \mathbf{P} \rangle|$ and $|\langle \mathbf{F}_q \rangle|$ will be strong, but even if the qubit is surrounded symmetrically by the TLSs, fluctuations will still give some correlation in a given sample. Small $|\langle \mathbf{P} \rangle|$ comes from cancellation in the directions of the individual moments.

There is an additional temperature scale associated with the interactions, which is the average change in the interaction energy from flipping one spin: $T_{\text{int}} = |\langle H_{\text{int}} \rangle| / Nk_B$. If $T_{\text{int}} < T^+, T^-$, then the interactions will turn off before the random-field effects as T is increased, and $|\langle \mathbf{P} \rangle|$ increases. If $T_{\text{int}} \gg T^+, T^-$, then the system is frozen by the interactions, and we expect little change in $|\langle \mathbf{P} \rangle|$ until $T \gg T_{\text{int}}$.

Overall, the effect of interactions is to make cancellation more likely due to their antiferromagnetic character. Unless the interactions are extremely strong, they make the nonmonotonic T dependence of $|\langle \mathbf{F}_q \rangle|$ and therefore of $\Delta f(T)$ more likely.

IV. CALCULATION DETAILS

This analytic analysis of the IRGM is semiquantitative. To make the arguments more firm we perform numerical simulations. We do this for three different physical pictures of the TLSs. In all simulations there is a single qubit at the origin.

In the first picture the TLSs are charge traps near the surface of a two-dimensional electron gas. The trap is positively charged when empty and then relatively negatively charged when full. We include the image charge. This can be described as a fluctuating dipole in the z direction, with z being the

growth direction. There are 30 dipoles uniformly distributed at positions $\mathbf{r}_j = (x_j, y_j, z_j)$, with $-150 < x_j, y_j < 150$ nm and $z_j = 50$ nm, thus in a layer of zero thickness above the qubit with an areal density of $3.33 \times 10^{-4}/\text{nm}^2$. This is the trap picture.

The second picture conceives of the TLSs as point defect dipoles in the oxide with orientations uniformly distributed in direction. The positions of the 30 TLSs $\mathbf{r}_j = (x_j, y_j, z_j)$ are uniformly distributed in a layer with coordinates satisfying $\mathbf{r}_j = (x_j, y_j, z_j)$, with $-150 < x_j, y_j < 150$ nm and $30 < z_j < 50$ nm. Thus, the TLSs are all located in a layer 20 nm thick with the center of the plane 30 nm above the qubit, with a density of $1.67 \times 10^{-5}/\text{nm}^3$. This is the random dipole picture.

In the third picture the 30 TLSs are distributed in the neighborhood of the qubit. The spatial positions of the TLSs are uniformly distributed in a spherical shell with the qubit at the center. $\mathbf{r}_j = (r_j, \theta_j, \phi_j)$ satisfy $60 < r_j < 80$ nm, $0 \leq \theta_j < \pi$, and $0 \leq \phi_j < 2\pi$. The radii are chosen to make $T_{\text{int}} \sim 1$ K. The density is $2.42 \times 10^{-5}/\text{nm}^3$. This is the spherical shell picture.

We define a random-field temperature scale $T_r = |\langle H_r \rangle| / Nk_B$ in addition to T_{int} . We use the parameter values $p_0 = 48 \text{ D} \approx 1|e| \text{ nm}$ and $N = 30$, which are chosen because they give T_2 of the order of 10^{-6} s in the correct experimental range [28]. The TLS density from these values is also consistent with those computed from the magnitude of measured power spectra [29,30]. It is desirable to sample values of the dipole strength p_0 from a distribution with variable mean and width. However, that would require a great increase in computation time. The random-field strength is taken as $\Delta E_0 = 5 \times 10^3 \text{ V/m}$, which denotes the standard deviation of a distribution centered on zero. With these values, $T_r \sim 0.1$ K, and $T_{\text{int}} \sim 1$ K in most samples, but while T_r is almost independent of the disorder because its strength is roughly fixed, T_{int} can vary from 0.1 to 10 K because it depends sensitively on the separations and orientations of the TLSs. Overall, these values are chosen to be representative of experiments on semiconductor qubit systems in the sense that most analyses give something like our value for N , which, together with the value of p_0 that we use, gives a reasonable dephasing time. A key observation here is that T_{int} comes out approximately correct when the distances of the TLSs from each other and from the qubit and the dipole magnitude are chosen to fit T_2 and other noise experiments. Further details are given in Appendix A. The IRGM passes the self-consistency check that T_{int} does, indeed, match the temperature scale at which Δf varies.

The number used for $|p_0|, 1|e| \text{ nm}$, means that the electron must hop three to four lattice spacings. This is a long distance on the atomic scale, but if the hopping is slow, the distance must, in fact, be long. This insight is at the basis of the theory of variable-range hopping conduction [31]. Experiments on this type of conduction at the Si-SiO₂ interface indeed showed hops of at least up to 3 nm [32]. In those experiments the interface was doped with Na impurities, but the localization length was independent of the impurity concentration, suggesting that the disorder is largely intrinsic. We do not propose that the noise in semiconductor devices arises from variable-range hopping, which seems unlikely to give telegraph noise. Rather, we cite the observation of such systems

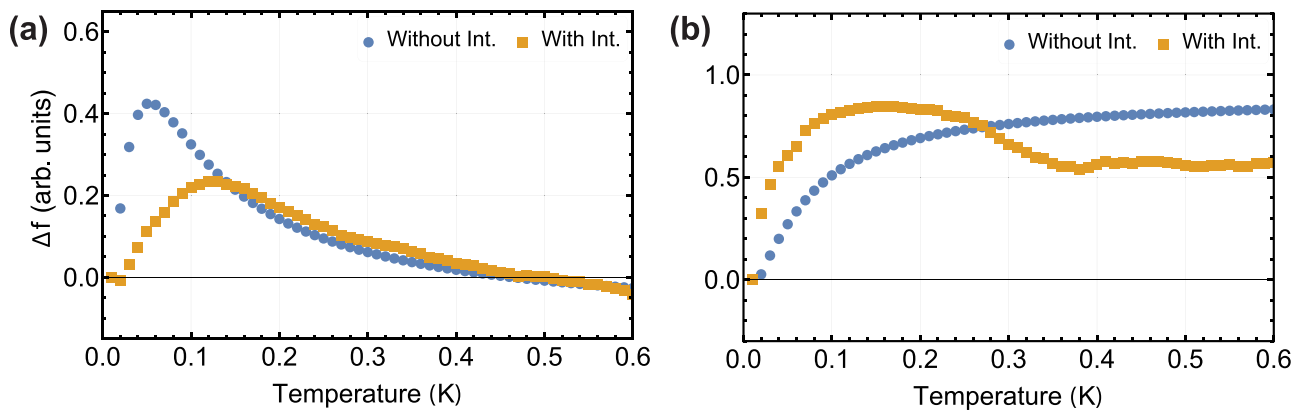


FIG. 1. Temperature dependence of qubit frequency shifts in the trap picture of the TLSs in some representative samples. The shifts are proportional to one component of the equilibrium electric field $\langle \mathbf{F}_q \rangle(T)$ at the qubit. “Without Int.” and “With Int.” indicate the noninteracting and fully interacting cases, respectively. (a) Both noninteracting and interacting cases show nonmonotonic shifts. (b) Example in which the interaction causes nonmonotonic behavior.

as an existence proof of long electron hops in disordered insulators.

We note that a much smaller value for the dipole magnitude is appropriate for dipole glasses in alloys of molecules with permanent dipole moments. An important recent paper [24] used a model of this kind. For example, in $(\text{KBr})_{1-x}(\text{KCN})_x$ the dipole moment of the TLSs is 0.2 D [33,34]. In a case like this the elastic interactions among the dipoles may be as strong as, or even stronger than, the Coulomb interaction that is dominant in electron tunneling models such as that employed here.

V. RESULTS

In Fig. 1 we plot one example of $\Delta f(T)$ in the trap picture for both the noninteracting case $H_{\text{int}} = 0$, which is exactly solvable, and the fully interacting case, which is computed by a Monte Carlo algorithm. Full details of the Monte Carlo simulations are given in Appendix E. The main physical point is that the TLSs can be thought of as being in thermal equilibrium in the experiment in Ref. [18] since they let the system thermalize for several minutes for each dataset.

We use arbitrary units for Δf since the conversion factor \mathbf{c}_q is platform dependent. For the interacting case, a moving average over 11 neighboring temperatures is applied to obtain stable results, and a smaller number of neighboring temperatures are used for the moving average at the ends of the curves.

We stress that $\langle \mathbf{F}_q \rangle(T)$ is sample dependent for all three pictures in that changing the parameters in natural ranges can alter $\Delta f(T)$ qualitatively. In particular, nonmonotonic behavior of $\langle \mathbf{F}_q \rangle$ is by no means universal. For a single sample it is even possible that one component of the field is nonmonotonic and another is monotonic. Some idea of the variety of possible behaviors is given in Appendix B.

Figure 1 demonstrates that nonmonotonicity can arise already even when the TLSs do not interact. This comes simply from the fact that there can be a cancellation of the random fields at $T = 0$ that is lessened as T increases in certain circumstances, as explained above. The interactions tend to enhance nonmonotonicity as in Fig. 1(a), although this effect is not universal. In fact, as we will see below, only a

minority of samples for the trap picture show nonmonotonicity. Interactions can create nonmonotonicity when the noninteracting picture shows monotonicity, as seen in Fig. 1(b). Again, this is consistent with the idea of cancellation as the active ingredient in nonmonotonicity. Additional examples of the different types of behavior that can occur for $\Delta f(T)$ are given in Appendix B.

Once universality of the nonmonotonicity is ruled out, the question becomes whether it is likely or not. To answer this we did simulations over 10 000 samples for each of the three pictures and determined whether a monotonic or nonmonotonic behavior was observed for each component of the electric field. The precise criterion for monotonicity or its absence is given in Appendix C.

The results in Table I support the physical picture explained above. In the trap picture, the cancellation of fields from different dipoles is relatively small since the vectors leading from the qubit to the TLSs, while not collinear, generally do not make large angles with each other. Similar statements apply to the random dipole picture, but there is some additional cancellation due to the different orientations. The most interesting result is for the spherical shell picture. Here we see the appearance of nonmonotonic behavior for noninteracting TLSs in about one quarter of the cases, as would be suggested by the above arguments. With dipoles on all sides of the qubit, the cancellation effect is quite strong.

Interactions do promote nonmonotonicity in all cases, as expected, especially when the interactions are strong: $T_{\text{int}} > T_r$. Overall, nonmonotonicity increases as we proceed from the trap to the random dipole to the spherical shell pictures. The interaction enhancement reinforces this pattern of nonmonotonicity.

We turn now to a comparison of theory and experiment. In nearly all measurements Δf is measured as a function of time, not temperature. Making a comparison to data of this type would require detailed modeling of the heat flow in the system, which is outside the scope of this paper. We therefore make a comparison only to the temperature data for $\Delta f(T)$ for six qubits in a single device reported in Ref. [18]. We plot these data with a theoretical fit in Fig. 2. The fit was done as follows. We first chose a set of TLS positions and

TABLE I. The fractional number of samples showing nonmonotonicity obtained from Monte Carlo simulation and exact solutions for three physical pictures. $\langle F_{q,i} \rangle$ is the i component of the vector $\langle \mathbf{F}_q \rangle(T)$. “Without Int.” and “With Int.” indicate the noninteracting and fully interacting cases, respectively. $T_r < T_{\text{int}}$ indicates $T_r \sim 0.1$ K and $T_{\text{int}} \sim 1$ K, while $T_r \sim T_{\text{int}}$ indicates $T_r \sim 0.1$ K and $T_{\text{int}} \sim 0.1$ K. The averages are taken over 10^4 samples.

Trap	$\langle F_{q,x} \rangle$	$\langle F_{q,y} \rangle$	$\langle F_{q,z} \rangle$
	$T_r < T_{\text{int}}$		
Without Int.	15.9%	16.4%	12.0%
With Int.	48.0%	48.6%	40.1%
	$T_r \sim T_{\text{int}}$		
Without Int.	11.0%	10.9%	7.4%
With Int.	30.5%	30.2%	24.2%
Random dipole	$\langle F_{q,x} \rangle$		
	$T_r < T_{\text{int}}$		
Without Int.	14.7%	15.9%	12.4%
With Int.	61.9%	61.9%	57.2%
	$T_r \sim T_{\text{int}}$		
Without Int.	10.0%	9.4%	7.8%
With Int.	42.5%	42.3%	36.9%
Spherical shell	$\langle F_{q,x} \rangle$		
	$T_r < T_{\text{int}}$		
Without Int.	25.0%	25.3%	28.0%
With Int.	89.5%	89.4%	90.1%
	$T_r \sim T_{\text{int}}$		
Without Int.	21.0%	21.8%	25.8%
With Int.	79.4%	79.0%	81.4%

random fields such that the parameters were in a range where nonmonotonicity could be expected and peak in Δf would be around 250 mK. Then, since the curves have a fairly similar shape but differ in vertical scale, we varied \mathbf{c}_q for each of the curves. Finally, the positions of the TLSs were adjusted to fit each curve individually. The main feature that needed to be accounted for in this final step was the sharper peak and

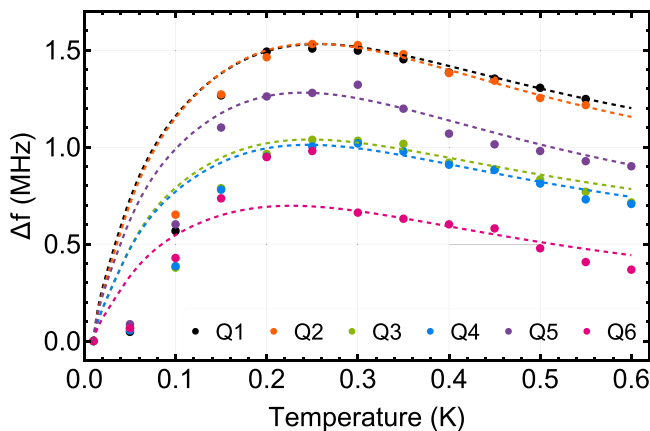


FIG. 2. PIRS data: theory and experiment. The points are measured frequency shifts for six qubits, Q1–Q6, from Ref. [18], and the dashed lines are theoretical fits. The qubits are situated in a one-dimensional array. The fitting procedure is described in detail in the text. The applied magnetic field is assumed to be in the y direction.

steeper falloff at high T that are seen in qubits 3–6. Some further details are given in Appendix D.

The fits are quite good quantitatively, but not too much should be made of this since the number of parameters far exceeds the number of qualitative features to be fit for each curve. However, even given this, the fit does provide evidence for the correctness of the IRGM. The nonmonotonicity arises naturally but also from the linear behavior at small T (which is caused by the uniform distribution of \mathbf{E}_j near zero) and, finally, the $1/T$ behavior at large T .

VI. CONCLUSION

We conclude by summarizing the strong and weak points of the IRGM as a model for PIRS. There are three evaluation categories: qualitative phenomenological understanding, semiquantitative self-consistency, and quantitative fit of the theory and experiment.

In qualitative terms, the surprising nonmonotonic T dependence and some of the other features of the T dependence of the qubit frequencies find a natural explanation in the IRGM. The important theoretical ingredients are the cancellations due to vector summations that involve only a relatively small number of variables combined with the natural temperature dependence of the TLS fluctuations and the depolarizing effects of interactions. The explanation of nonmonotonicity quite defies the usual expectation that thermal effects in the absence of phase transitions tend to be monotonic. Overall, this is quite strong evidence for the IRGM. Aside from the nonmonotonicity, there is the observation that Δf is sometimes negative [16,19]. This is also somewhat surprising if one assumes that the heating affects the qubits directly in some fashion. In the IRGM, there is nothing that constrains the sign of the components of \mathbf{c}_q , so the sign of the effect is not determined. Similarly, the fact that the effect is not resonant with qubit frequencies suggests that an ancillary part of the device is driven by the heating; in the IRGM, the system of TLSs is driven. Hysteresis does not seem to be a feature of PIRS. This might seem to argue against the IRGM, but in fact, with only a few tens of TLSs involved, this aspect of glassiness does not argue against the model. In contrast, no T -dependent electric field shows up in measurements at the charge sensor [18], which is not explained in the model as it stands.

There are two experimental scales that must be consistent with the theory: the overall magnitude of Δf (1 MHz in dot systems) and the temperature of the peak in Δf (about 0.2 to 0.4 K in dot systems). The first number is very consistent with the roughly known numbers for the magnitude of the moment of the dipoles and their presumed positions. The second depends on the distribution of the random local fields \mathbf{E}_j , and indeed, the distribution must be such that $|p_0 \mathbf{E}_j / k_B|$ is clustered near 0.3 K. There is no obvious reason why this should be so, so the IRGM does include at least one *ad hoc* element.

The fit to the data in Fig. 2 is strikingly accurate, but it raises questions. If interactions are relatively weak for some reason (such that the TLSs are particularly far apart), then why do six out of six qubits all show nonmonotonicity? This is only consistent with the spherical shell picture, which in turn is not very consistent with the usual idea that the TLSs are

associated with the oxide layer. Furthermore, the nonmonotonicity in all six qubits means that there must be correlations between the positions of the TLSs and the strength and direction of their random fields. Specifically, the TLSs closer to the qubits must have stronger random fields for each qubit. In addition, in order for the shift to be positive in all qubits, the random fields for the nearby TLSs must all have the same orientation across all six qubits.

We conclude that the basic mechanism of PIRS is explained by the IRGM but that the explanation is far from complete at this stage. Most likely, the model needs to be supplemented by a better picture of the positions of the TLSs and a better understanding of their physical nature. This would limit the model to a smaller region of its parameter space and give it more explanatory power. Thus, for example, if the random-field strength and the electric field of the TLSs are correlated in the appropriate way for reasons that have not yet emerged, the nonmonotonicity would become a universal feature.

ACKNOWLEDGMENTS

We acknowledge helpful discussions and correspondence with S. N. Coppersmith, M. A. Eriksson, M. Friesen, A. Laucht, A. Morello, A. Saraiva, L. M. K. Vandersypen, and H. Yang. This research was sponsored by the Army Research Office (ARO) under Awards No. W911NF-17-1-0274 and No. W911NF-23-1-0110. This research was performed using the computer resources and assistance of the UW-Madison Center for High Throughput Computing (CHTC) in the Department of Computer Sciences.

The views, conclusions, and recommendations contained in this document are those of the authors and are not necessarily endorsed nor should they be interpreted as representing the official policies, either expressed or implied, of the Army Research Office (ARO) or the U.S. Government. The U.S. Government is authorized to reproduce and distribute reprints for Government purposes notwithstanding any copyright notation herein.

APPENDIX A: MAGNITUDE OF FREQUENCY SHIFT IN QUANTUM DOT ARCHITECTURE

Here we give an order-of-magnitude estimate of the PIRS effect and some of the intermediate quantities involved in it for a Si/SiGe heterostructure quantum dot device with a micromagnet. In this case, Δf is due to the shift in position of the electron in the nonuniform magnetic field caused by the micromagnet. Let there be an electron spin qubit in a quantum dot at the origin of coordinates. The electron is at the bottom of a circularly symmetric two-dimensional harmonic potential $k(x^2 + y^2)/2$. At this point there is a magnetic field gradient $\partial B_i/\partial x_j$, where i and j are Cartesian indices. The static electric field of the TLSs moves the qubit in the gradient and therefore changes the magnetic field on the spin.

The qubit frequency shift is determined by $\Delta f = \mathbf{c}_q \cdot [\langle \mathbf{F}_q \rangle(T) - \langle \mathbf{F}_q \rangle(T = 0)]$, with the frequency susceptibility \mathbf{c}_q given as [28]

$$\mathbf{c}_q = \frac{g\mu_B}{h} \frac{q}{m_i \omega_{\text{orb}}^2} \left(\frac{\partial B_y}{\partial x} \hat{x} + \frac{\partial B_x}{\partial y} \hat{y} \right). \quad (\text{A1})$$

We have assumed that the externally applied magnetic field is in the y direction. A typical device of this kind that was particularly well characterized was described in Ref. [35]. The magnetic field gradients for that device in units of $\text{mT}(\text{nm})^{-1}$ were $\partial B_y/\partial x = -0.05$ and $\partial B_y/\partial y = 0.18$. The transverse effective mass $m_i = 0.19 m_e = 1.73 \times 10^{-31}$ kg. We take the lowest orbital excitation frequency as $\omega_{\text{orb}} \sim 2 \text{ meV}/\hbar$, which is related to the spring constant by $k = m_i \omega_{\text{orb}}^2$, and an average value of $|\nabla B|$ of $0.1 \text{ mT}(\text{nm})^{-1}$. These numerical values should be more or less typical of micromagnet-based Si/SiGe devices, but variations from device to device could certainly alter our estimate.

A single component of $\langle \mathbf{F}_q \rangle$ at $T = 0$ is the result of a random-walk summation of the same component of the field exerted at the position of the qubit by the N TLSs. It is therefore given by \sqrt{N} times the rms value of the individual contributions to one component in the sum in Eq. (A1). There is an additional angular average over the directions of \mathbf{p}_i with the result that $\Delta f(T = 0) \sim \sqrt{2N/3} p_0/4\pi \epsilon_r d^3$, where d is an average distance from the TLSs to the qubit, and we use $d \sim 50 \text{ nm}$ and $\epsilon_r \sim 11$. Combining this with Eq. (A1), we find $\Delta f(T = 0) \sim 1.4 \text{ MHz}$, not too far from what is observed for the maximum Δf , which should be roughly comparable with the computed quantity. With these parameters, the qubit moves about 0.5 nm due to $\langle \mathbf{F}_q \rangle$, a field of about 4500 V/m .

APPENDIX B: FURTHER EXAMPLES OF THE TEMPERATURE DEPENDENCE OF THE ELECTRIC FIELD

In this Appendix we give a few representative examples of the temperature dependence of the qubit frequency for single TLS configurations in the different pictures of TLS positions and directions. In each figure we show two configurations with the interaction turned off and on. In fact, we compute the y component of $\langle \mathbf{F}_q \rangle$ and leave $\mathbf{c}_{q,y}$ arbitrary. Then we enforce the condition that $\Delta f(T = 0) = 0$. This means that the ground state configurations for the interacting and noninteracting cases and their resultant $\langle \mathbf{F}_q \rangle$ may be quite different. The curves for the interacting case are smoothed by averaging over the 11 points centered at the plotted point, except at the ends of the curve. Note that $\langle \mathbf{F}_q \rangle \rightarrow 0$ as $T \rightarrow \infty$, but this asymptote is usually off the plotted region.

In Fig. 3 we plot results for the random dipole picture. Figure 3(a) shows an example in which T^+ considerably exceeds T^- , leading in the noninteracting case to a peak at relatively low T . Interactions mainly shift the peak but leave nonmonotonicity intact. In Fig. 3(b) the needed cancellation pattern does not occur for the noninteracting case, but there is nonmonotonicity in the interacting case because of increased cancellation. Interactions have a strong influence on the ground state configuration for this particular sample, as indicated by the change in sign for the interacting and noninteracting cases.

In Fig. 4 we see $\Delta f(T)$ for the spherical shell picture for two different TLS configurations. In this picture the interactions are more effective in producing nonmonotonicity, and once more, we see that the nonmonotonicity can be present already in the noninteracting case or it can be induced by the

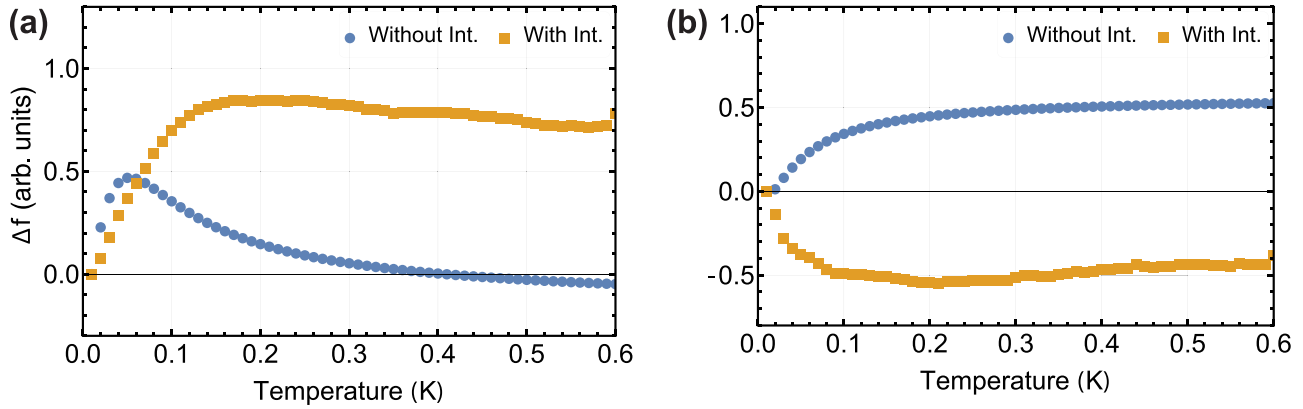


FIG. 3. Temperature dependence of qubit frequency shifts in the random dipole picture of the TLSs. The shifts are computed from the equilibrium electric field $\langle \mathbf{F}_q \rangle(T) - \langle \mathbf{F}_q \rangle(T=0)$ at the position of the qubit for two configurations of the TLSs. “Without Int.” and “With Int.” indicate the noninteracting ($H_{\text{int}} = 0$) and fully interacting cases, respectively. (a) Both the noninteracting and interacting cases show nonmonotonic shifts. (b) Example in which the interaction causes nonmonotonic behavior. The applied magnetic field is assumed to be in the y direction.

interactions. $\Delta f(T)$ can show somewhat surprising behavior in the interacting case, in which it has a more complicated increase and decrease as a function of T . This has not been observed to date. If it were, it would be a sign that interactions are important.

In Fig. 5 we plot $\Delta f(T)$ for two samples belonging to the trap and random dipole pictures. These plots are mainly included to dispel any impression that nonmonotonicity is universal in the IRGM. Both the noninteracting and interacting cases can show monotonic behavior as a function of temperature. This can happen as in Fig. 5(a), where the ground state configuration of the TLSs changes drastically when interactions are turned on, or as in Fig. 5(b), where the two ground states are apparently rather similar.

APPENDIX C: NONMONOTONICITY CRITERION

To determine whether a component $F_{q,i}(T)$ of $\langle \mathbf{F}_q \rangle$ has nonmonotonic T dependence, we set up the following criterion: from exact or numerical results, we define a set of

differences

$$F_{\text{diff}} = \{F_{m+1} - F_m \mid m = 1, 2, 3, \dots, M-1\}, \quad (\text{C1})$$

where $M = 100$ is the number of temperature points for evaluation. The average slope magnitude is defined as

$$s = \frac{1}{M-1} \sum_{m=1}^{M-1} |F_{m+1} - F_m|. \quad (\text{C2})$$

To avoid false positives from small random fluctuations (which is particularly important for Monte Carlo simulations), small slope elements are excluded from F_{diff} so that the smaller set is

$$F_{\text{large}} = \left\{ F_{m+1} - F_m \mid \frac{s}{2} < |F_{m+1} - F_m| \right\}. \quad (\text{C3})$$

Defining the signs of the differences as $\sigma_m = \text{sgn}(F_{m+1} - F_m)$, we have groups of positive and negative slopes:

$$\begin{aligned} F_{\text{pos}} &= \{F_{m+1} - F_m \mid \sigma_m > 0 \text{ and } F_{m+1} - F_m \in F_{\text{large}}\}, \\ F_{\text{neg}} &= \{F_{m+1} - F_m \mid \sigma_m < 0 \text{ and } F_{m+1} - F_m \in F_{\text{large}}\}. \end{aligned} \quad (\text{C4})$$

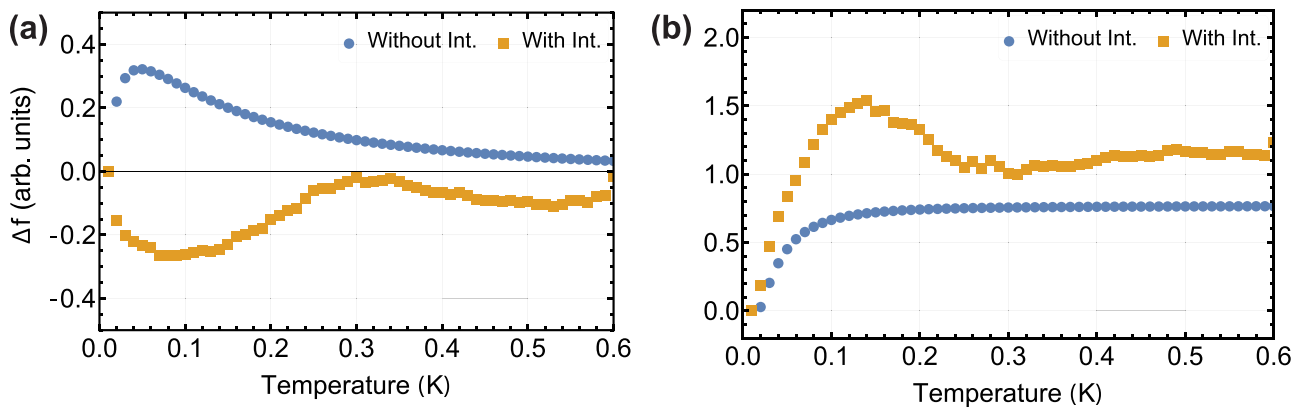


FIG. 4. Temperature dependence of qubit frequency shifts in the spherical shell picture of the TLSs. The shifts are computed from the equilibrium electric field $\langle \mathbf{F}_q \rangle(T) - \langle \mathbf{F}_q \rangle(T=0)$ at the position of the qubit for two configurations of the TLSs. “Without Int.” and “With Int.” indicate the noninteracting ($H_{\text{int}} = 0$) and fully interacting cases, respectively. (a) Both the noninteracting and interacting cases show nonmonotonic shifts. (b) Example in which interaction causes nonmonotonic behavior. The applied magnetic field is assumed to be in the y direction. Note the change in vertical scale from (a) to (b).

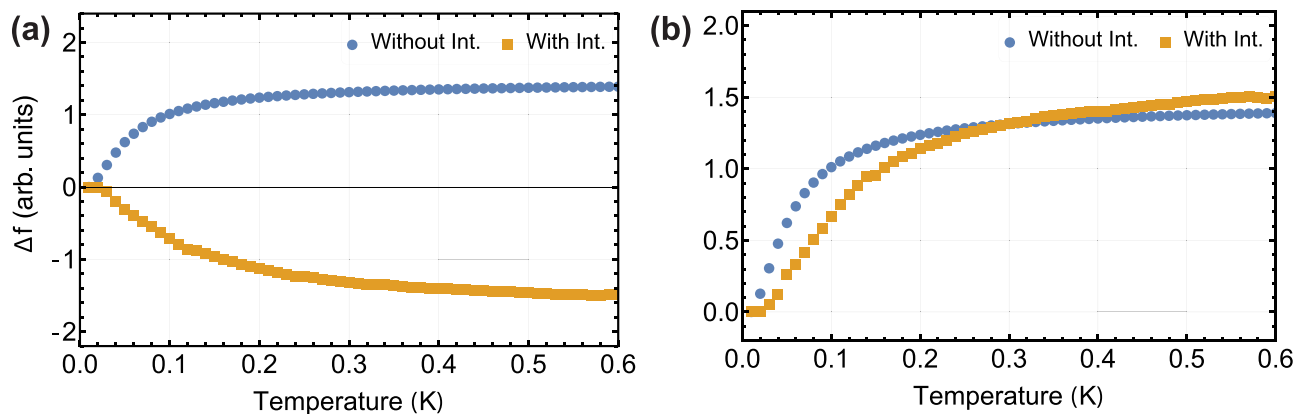


FIG. 5. Temperature dependence of qubit frequency shifts in the trap and random dipole picture of the TLSs. The shifts are computed from the equilibrium electric field $\langle \mathbf{F}_q \rangle(T) - \langle \mathbf{F}_q \rangle(T=0)$ at the position of the qubit for two configurations of the TLSs. “Without Int.” and “With Int.” indicate the noninteracting ($H_{\text{int}} = 0$) and fully interacting cases, respectively. Both the noninteracting and interacting cases show monotonic shifts for the (a) trap and (b) random dipole pictures. The applied magnetic field is assumed to be in the y direction. Note the change in vertical scale from (a) to (b).

The final nonmonotonicity criterion is

$$\frac{\min(|F_{\text{pos}}|, |F_{\text{neg}}|)}{|F_{\text{pos}}| + |F_{\text{neg}}|} > 0.1, \quad s > 5, \quad (\text{C5})$$

where the first inequality requires that $F_{q,i}(T)$ has non-negligible positive and negative parts of slopes and the second one demands that the overall frequency shift in the temperature range is not so small. The tolerance values, 0.1 and 5, are empirically chosen and can be adjusted for different systems.

APPENDIX D: FITTING PROCEDURE FOR FIGURE 2

In Fig. 2 of the main text we give a comparison of theory and the PIRS experiment of Undseth *et al.* [18] in which Δf was measured for each of six qubits in a row. We found that the best fit is obtained by taking the case that $T_r \gg T_{\text{int}}$, which amounts to a noninteracting model. We used a trap picture, but the other two pictures could also have been used for the fit. The parameters are the same as those in the description of the trap picture in the main text except for the z coordinates of the TLSs, which are now taken as $z_j = 36$ nm following Refs. [1, 18], and $\Delta E_0 = 5 \times 10^4$ V/m. The six samples are generated by varying the conversion factor $\mathbf{c}_{q,y}$ and the positions of TLSs in the x - y plane, which are randomly assigned within circles whose centers are TLS positions of a reference sample and radii are 5 nm. The applied magnetic field is assumed to be in the y direction. As we showed in Appendix A, the order of magnitude of the effect is consistent between theory and experiment. The best fit for the conversion factors for the qubits Q_i , with $i = 1, 2, 3, 4, 5, 6$, was in the ratio 0.105:0.114:0.072:0.077:0.103:0.059. All fit parameters are available from the authors on request.

APPENDIX E: MONTE CARLO SIMULATIONS

$\langle \mathbf{F}_q(T) \rangle$, the quantity plotted in Figs. 1 and 2 in the main text, is calculated by Monte Carlo simulations. We use Eq. (1), where one averages over sets of spin configurations s_j which are drawn from thermal ensembles generated by the simulation. The spatial positions \mathbf{r}_j of the spins form random lattices in accord with the probability distributions specified in Sec. IV for the three pictures envisioned. The probability distribution of the random field \mathbf{E}_j is a Gaussian for each component with zero mean, and its standard deviation is 5×10^3 V/m for $T_r \sim 0.1$ K and 5×10^4 V/m for $T_r \sim 1$ K. For each point in Figs. 1 and 2 we average over 10^4 samples. The number of TLSs in each sample is 30. Free boundary conditions are used, which is necessary for the geometries investigated. The Metropolis algorithm is used. The simulations are started at the given temperature and equilibrated with a “spin-up” period to let the energy converge. We require that the system energy has leveled off (converged), and the convergence criterion is that the excursions of the total energy of the system are of the order of the change in energy caused by a single spin flip. The data from the spin-up period are discarded. The spins are flipped at random rather than cycling through the spins in order. A flip is accepted with probability $\exp(-\Delta H/k_B T) / [1 + \exp(-\Delta H/k_B T)]$, where ΔH is the change in energy caused by the spin flip. The number of Monte Carlo steps (attempted number of flips divided by the number of spins) for each sample is $S = 3333$. These relatively short simulation times make it possible to analyze the large number of samples needed for disorder averaging. The short times give reliable results because the number of spins is small.

[1] S. G. Philips, M. T. Mądzik, S. V. Amitonov, S. L. de Snoo, M. Russ, N. Kalhor, C. Volk, W. I. Lawrie, D. Brousse, L. Tryputen, B. Paquelet Wuetz, A. Sammak, M. Veldhorst, G.

Scappucci, and L. M. K. Vandersypen, Universal control of a six-qubit quantum processor in silicon, *Nature (London)* **609**, 919 (2022).

- [2] A. R. Mills, C. R. Guinn, M. J. Gullans, A. J. Sigillito, M. M. Feldman, E. Nielsen, and J. R. Petta, Two-qubit silicon quantum processor with operation fidelity exceeding 99%, *Sci. Adv.* **8**, eabn5130 (2022).
- [3] C. Dekker, A. J. Scholten, F. Liefink, R. Eppenga, H. van Houten, and C. T. Foxon, Spontaneous resistance switching and low-frequency noise in quantum point contacts, *Phys. Rev. Lett.* **66**, 2148 (1991).
- [4] K. Takeda, T. Obata, Y. Fukuoka, W. M. Akhtar, J. Kamioka, T. Kodera, S. Oda, and S. Tarucha, Characterization and suppression of low-frequency noise in Si/SiGe quantum point contacts and quantum dots, *Appl. Phys. Lett.* **102**, 123113 (2013).
- [5] Ç. Kurdak, C.-J. Chen, D. C. Tsui, S. Parihar, S. Lyon, and G. W. Weimann, Resistance fluctuations in GaAs/Al_xGa_{1-x} As quantum point contact and Hall bar structures, *Phys. Rev. B* **56**, 9813 (1997).
- [6] T. Sakamoto, Y. Nakamura, and K. Nakamura, Distributions of single-carrier traps in GaAs/Al_xGa_{1-x} As heterostructures, *Appl. Phys. Lett.* **67**, 2220 (1995).
- [7] C. Buizert, F. H. L. Koppens, M. Pioro-Ladrière, H.-P. Tranitz, I. T. Vink, S. Tarucha, W. Wegscheider, and L. M. K. Vandersypen, *In situ* reduction of charge noise in GaAs/AlGaAs Schottky-gated devices, *Phys. Rev. Lett.* **101**, 226603 (2008).
- [8] M. Pioro-Ladrière, J. H. Davies, A. R. Long, A. S. Sachrajda, L. Gaudreau, P. Zawadzki, J. Lapointe, J. Gupta, Z. Wasilewski, and S. Studenikin, Origin of switching noise in GaAs/Al_xGa_{1-x}As lateral gated devices, *Phys. Rev. B* **72**, 115331 (2005).
- [9] J. Campbell and P. Lenahan, Density of states of Si/SiO₂ interface trap centers, *Appl. Phys. Lett.* **80**, 1945 (2002).
- [10] X. G. Croot, S. J. Pauka, M. C. Jarratt, H. Lu, A. C. Gossard, J. D. Watson, G. C. Gardner, S. Fallahi, M. J. Manfra, and D. J. Reilly, Gate-sensing charge pockets in the semiconductor-qubit environment, *Phys. Rev. Appl.* **11**, 064027 (2019).
- [11] E. Paladino, Y. M. Galperin, G. Falci, and B. L. Altshuler, $1/f$ noise: Implications for solid-state quantum information, *Rev. Mod. Phys.* **86**, 361 (2014).
- [12] E. J. Connors, J. J. Nelson, H. Qiao, L. F. Edge, and J. M. Nichol, Low-frequency charge noise in Si/SiGe quantum dots, *Phys. Rev. B* **100**, 165305 (2019).
- [13] E. J. Connors, J. Nelson, L. F. Edge, and J. M. Nichol, Charge-noise spectroscopy of Si/SiGe quantum dots via dynamically-decoupled exchange oscillations, *Nat. Commun.* **13**, 940 (2022).
- [14] J. M. Boter, X. Xue, T. Krähenmann, T. F. Watson, V. N. Premakumar, D. R. Ward, D. E. Savage, M. G. Lagally, M. Friesen, S. N. Coppersmith, M. A. Eriksson, R. Joynt, and L. M. K. Vandersypen, Spatial noise correlations in a Si/SiGe two-qubit device from Bell state coherences, *Phys. Rev. B* **101**, 235133 (2020).
- [15] J. Rojas-Arias, A. Noiri, P. Stano, T. Nakajima, J. Yoneda, K. Takeda, T. Kobayashi, A. Sammak, G. Scappucci, D. Loss, and S. Tarucha, Spatial noise correlations beyond nearest-neighbor in ²⁸Si/SiGe spin qubits, *Phys. Rev. Appl.* **20**, 054024 (2023).
- [16] K. Takeda, J. Yoneda, T. Otsuka, T. Nakajima, M. Delbecq, G. Allison, Y. Hoshi, N. Usami, K. M. Itoh, S. Oda, T. Kodera, and S. Tarucha, Optimized electrical control of a Si/SiGe spin qubit in the presence of an induced frequency shift, *npj Quantum Inf.* **4**, 54 (2018).
- [17] T. F. Watson, S. G. J. Philips, E. Kawakami, D. R. Ward, P. Scarlino, M. Veldhorst, D. E. Savage, M. G. Lagally, M. Friesen, S. N. Coppersmith, M. A. Eriksson, and L. M. K. Vandersypen, A programmable two-qubit quantum processor in silicon, *Nature (London)* **555**, 633 (2018).
- [18] B. Undseth, O. Pietx-Casas, E. Raymenants, M. Mehmandoost, M. T. Mądzik, S. Philips, S. de Snoo, D. Michalak, S. Amitonov, L. Tryputen, B. Wuetz, V. Fezzi, D. Esposti, A. Sammak, G. Scappucci, and L. Vandersypen, Hotter is easier: Unexpected temperature dependence of spin qubit frequencies, *Phys. Rev. X* **13**, 041015 (2023).
- [19] A. Zwerver *et al.*, Qubits made by advanced semiconductor manufacturing, *Nat. Electron.* **5**, 184 (2022).
- [20] S. Freer, S. Simmons, A. Laucht, J. T. Muhonen, J. P. Dehollain, R. Kalra, F. A. Mohiyaddin, F. E. Hudson, K. M. Itoh, J. C. McCallum, D. N. Jamieson, A. S. Dzurak, and A. Morello, A single-atom quantum memory in silicon, *Quantum Sci. Technol.* **2**, 015009 (2017).
- [21] R. Savytskyy, T. Botzem, I. F. de Fuentes, B. Joecker, F. E. Hudson, K. M. Itoh, A. M. Jakob, B. C. Johnson, D. N. Jamieson, A. S. Dzurak, and A. Morello, An electrically-driven single-atom ‘flip-flop’ qubit, *Sci. Adv.* **9**, eadd9408 (2023).
- [22] G. Chen, Non-Fourier phonon heat conduction at the microscale and nanoscale, *Nat. Rev. Phys.* **3**, 555 (2021).
- [23] L. Lindsay, First principles Peierls-Boltzmann phonon thermal transport: A topical review, *Nanoscale Microscale Thermophys. Eng.* **20**, 67 (2016).
- [24] D. L. Mickelsen, H. M. Carruzzo, S. N. Coppersmith, and C. C. Yu, Effects of temperature fluctuations on charge noise in quantum dot qubits, *Phys. Rev. B* **108**, 075303 (2023).
- [25] C. Müller, J. Lisenfeld, A. Shnirman, and S. Poletto, Interacting two-level defects as sources of fluctuating high-frequency noise in superconducting circuits, *Phys. Rev. B* **92**, 035442 (2015).
- [26] C. Müller, J. H. Cole, and J. Lisenfeld, Towards understanding two-level-systems in amorphous solids: Insights from quantum circuits, *Rep. Prog. Phys.* **82**, 124501 (2019).
- [27] R. Rahman, S. H. Park, T. B. Boykin, G. Klimeck, S. Rogge, and L. C. L. Hollenberg, Gate-induced g-factor control and dimensional transition for donors in multivalley semiconductors, *Phys. Rev. B* **80**, 155301 (2009).
- [28] Y. Choi and R. Joynt, Anisotropy with respect to the applied magnetic field of spin qubit decoherence times, *npj Quantum Inf.* **8**, 70 (2022).
- [29] M. M. E. K. Shehata, G. Simion, R. Li, F. A. Mohiyaddin, D. Wan, M. Mongillo, B. Govoreanu, I. Radu, K. De Greve, and P. Van Dorpe, Modeling semiconductor spin qubits and their charge noise environment for quantum gate fidelity estimation, *Phys. Rev. B* **108**, 045305 (2023).
- [30] M. Kępa, Ł. Cywiński, and J. A. Krzywda, Correlations of spin splitting and orbital fluctuations due to $1/f$ charge noise in the Si/SiGe quantum dot, *Appl. Phys. Lett.* **123**, 034003 (2023).
- [31] N. F. Mott, *Conduction in Non-crystalline Materials*, Oxford Science Publications (Clarendon, Oxford, 1987).
- [32] G. Timp, A. B. Fowler, A. Hartstein, and P. N. Butcher, Hopping conduction in a two-dimensional impurity band, *Phys. Rev. B* **34**, 8771 (1986).
- [33] F. Lüty, Alkali-cyanides and their mixtures with alkali-halides: Model systems for the evolution of molecular order and phase transitions, in *Proceedings of the International Conference on*

- Defects in Insulating Crystals, Riga, 1981*, edited by V. M. Turkevich and K. D. Schwartz (Zinātne, Riga, 1981), p. 69.
- [34] C. C. Yu, Possible mechanism for thermal conductivity in $(\text{KBr})_{1-x}(\text{KCN})_x$, *Phys. Rev. B* **32**, 4220 (1985).
- [35] E. Kawakami, P. Scarlino, D. R. Ward, F. R. Braakman, D. E. Savage, M. G. Lagally, M. Friesen, S. N. Coppersmith, M. A. Eriksson, and L. M. K. Vandersypen, Electrical control of a long-lived spin qubit in a Si/SiGe quantum dot, *Nat. Nanotechnol.* **9**, 666 (2014).
- Correction:* A typographical error in one of the award numbers in the Acknowledgment section has been fixed.